Inorganic Chemistry

Article

pubs.acs.org/IC

# $K_4Fe_3F_{12}$: An $Fe^{2+}/Fe^{3+}$ Charge-Ordered, Ferrimagnetic Fluoride with a Cation-Deficient, Layered Perovskite Structure

Sun Woo Kim,[†] Ronghuan Zhang,[‡] P. Shiv Halasyamani,*[,†] and Michael A. Hayward*[,‡]

[†]Department of Chemistry, University of Houston, 112 Fleming Building, Houston, Texas 77204-5003, United States

[‡]Inorganic Chemistry Laboratory, Department of Chemistry, University of Oxford, South Parks Road, Oxford, OX1 3QR, United Kingdom

Supporting Information

**ABSTRACT:** A new mixed-valence iron ($Fe^{2+}/Fe^{3+}$) fluoride material with a layered perovskite-related structure has been synthesized and characterized. The material, $K_4Fe_3F_{12}$ [$K_4(Fe^{2+})(Fe^{3+})_2F_{12}$], was synthesized using mild hydrothermal conditions. The material exhibits a layered perovskite structure consisting of alternating sheets of apex-linked $Fe^{2+}F_6$ and $Fe^{3+}F_6$ octahedra; thus, each layer of $Fe^{2+}F_6$ centers is sandwiched between two layers of $Fe^{3+}F_6$ centers. Magnetization and neutron powder diffraction data show that, upon cooling below 120 K, $K_4Fe_3F_{12}$ adopts a magnetically ordered state in which the $Fe^{3+}$ and $Fe^{2+}$ spins are aligned in an approximately antiparallel manner to each other to yield a pseudoferrimagnetic structure with a net spontaneous moment of 5.41 $\mu_B$ per formula unit at 10 K. Crystal data: $K_4Fe_3F_{12}$, trigonal space group $R\bar{3}m$ (No. 166), $a = b = 5.7649(9)$ Å, $c = 28.086(9)$ Å, $V = 808.36(3)$ Å$^3$, $Z = 3$, $T = 296(2)$ K.

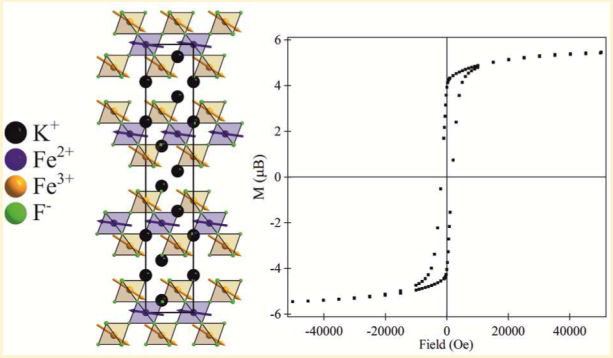


## INTRODUCTION

The discovery of new magnetic materials can be a cumbersome and inefficient process because many parameters (crystal structure, local magnetic moment, and magnetic coupling interactions) need to be controlled and optimized in order to prepare materials with desired properties and behaviors, and there is often little prior guidance as to how the chemical composition and synthesis conditions of the materials influence and control these parameters.

In an attempt to add a greater degree of design and control into the search for new functional magnetic materials, it is useful to observe that, in comparison to the more widely studied transition-metal oxides, the reduced anionic charge of the $F^-$ fluoride ion means that extended metal fluoride lattices contain metal cations in lower oxidation states than their oxide structural analogues. As a result, the transition-metal cations in extended fluoride lattices have higher d-electron counts than those in the equivalent oxide phases.

This feature of metal fluoride chemistry is particularly useful when preparing magnetic materials because there are many metal−anion frameworks that cannot easily accommodate paramagnetic transition-metal cations when the anion is oxide and the high metal oxidation states required to stabilize these oxide frameworks typically have $d^0$ diamagnetic electronic configurations.[1] When fluoride analogues of these oxide phases are prepared, transition-metal cations in much lower oxidation states, with paramagnetic non-$d^0$ electronic configurations, can be accommodated, allowing a range of novel paramagnetic materials to be prepared. For example, tetragonal tungsten bronze oxide phases such as $NaBa_2Nb_5O_{15}$ or $NaBa_2Ta_5O_{15}$[2] typically require diamagnetic $Nb^{5+}$ or $Ta^{5+}$ to stabilize them, while in contrast, structurally analogous fluoride phases such as $K_3Fe_5F_{15}$, $K_3Cu_2Fe_3F_{15}$, or $K_3Cr_3Fe_2F_{15}$[3−5] contain paramagnetic centers that couple to adopt ferrimagnetic and antiferromagnetic configurations at low temperature. When these magnetic behaviors are combined with the ferroelectric behavior of this lattice type, these fluoride materials become good candidates for the exhibition of multiferroic magnetoelectric coupling.

A further example of this phenomenon of a diamagnetic oxide lattice having a paramagnetic fluoride analogue can be seen in the layered "110" perovskite phases: diamagnetic $LnMO_4$ (Ln = lanthanide, M = Nb, Ta)[6−8] oxide phases have the same structural topology as paramagnetic $BaMF_4$ fluorides (M = Mn, Co, Ni).[9−12] In common with the tetragonal tungsten bronze phases, many of these "110" perovskite materials also adopt distorted, noncentrosymmetric lattices and exhibit ferroelectric behavior and potentially multiferroic coupling.

Given that the factors that govern the crystal structures adopted by metal oxides and metal fluorides are similar, many extended metal oxide phases are likely to have thermodynamically stable metal fluoride analogues. Thus, a more efficient

**Received:** May 5, 2015
**Published:** June 22, 2015





DOI: 10.1021/acs.inorgchem.5b01006
*Inorg. Chem.* 2015, 54, 6647−6652

method for the discovery of novel magnetic materials is the preparation of complex transition-metal fluoride phases based on known metal oxide frameworks because this adds a degree of predictability to the compositional/structural relations.

Here we describe the synthesis and magnetic behavior of $K_4Fe_3F_{12}$, a mixed-valence $Fe^{2+}/Fe^{3+}$ fluoride phase, which is the first fluoride analogue to a series of structurally analogous diamagnetic oxide phases.

## EXPERIMENTAL SECTION

**Reagents.** KF (Alfa Aesar, ACS 99%), $FeF_2$ (Alfa Aesar, 99%), $FeF_3$ (Alfa Aesar, 97%), and $CF_3COOH$ (Alfa Aesar, 99%) were used without any further purification.

**Synthesis.** $K_4Fe_3F_{12}$ was synthesized using a method described earlier for the phase pure synthesis of the multiferroic $BaMF_4$ family.[12] A total of 0.125 g ($2.15 \times 10^{-3}$ mol) of KF, 0.107 g ($1.14 \times 10^{-3}$ mol) of $FeF_2$, 0.129 g ($1.14 \times 10^{-3}$ mol) of $FeF_3$, and 3 mL ($3.90 \times 10^{-2}$ mol) of $CF_3COOH$ were combined with 5 mL of $H_2O$. The mixture was placed in a 23 mL Teflon-lined stainless steel autoclave that was closed and heated to 230 °C. The autoclave was heated for 24 h and cooled slowly to room temperature at a rate of 6 °C $h^{-1}$. The only solid product, brownish-yellow hexagonal plate-shaped crystals subsequently shown to be $K_4Fe_3F_{12}$, was recovered in 50% yield based on $FeF_2$.

**Single-Crystal X-ray Diffraction.** A brownish-yellow hexagonal plate-shaped crystal (0.04 × 0.03 × 0.01 mm) was selected for single-crystal data collection. The data were collected using a Siemens SMART APEX diffractometer equipped with a 1K CCD area detector using graphite-monochromated Mo K$\alpha$ radiation. A hemisphere of data was collected using a narrow-frame method with scan widths of 0.300 in $\omega$ and an exposure time of 40 s $frame^{-1}$. The data were integrated using the Siemens *SAINT* program,[13] with the intensities corrected for Lorentz polarization, air absorption, and absorption attributable to variation in the path length through the detector face plate. $\psi$ scans were used for absorption correction on the data. The data were solved and refined using *SHELXS-97* and *SHELXL-97*, respectively.[14,15] All of the atoms were refined with anisotropic thermal parameters and the refinement converged for $I > 2\sigma(I)$. All calculations were performed using the *WinGX-98* crystallographic software package.[16]

**Powder Diffraction.** Powder X-ray diffraction data were collected from $K_4Fe_3F_{12}$ using a PANalytical X'pert pro diffractometer (Cu K$\alpha$ radiation) in the range $5° < 2\theta < 70°$. Neutron powder diffraction data were collected from a finely ground sample (mass ~3 g) contained within a cylindrical vanadium can using the GEM diffractometer at the ISIS neutron source, Oxfordshire, U.K. Reitveld profile refinements were performed against these data using the *GSAS* suite of programs.[17]

**Magnetization Data.** Magnetization data were collected from finely ground powder samples using a Quantum Design MPMS SQUID magnetometer.

## RESULTS

**Structural Characterization.** Analysis of the single-crystal X-ray diffraction data reveals that $K_4Fe_3F_{12}$ adopts a layered, cation-deficient perovskite structure, analogous to that of $La_4Ti_3O_{12}$.[18] Full crystallographic data, atomic coordinates and thermal parameters, and selected bond distances and angles and bond valence sum (BVS) analysis for $K_4Fe_3F_{12}$ are given in Tables 1–3, respectively, with a representation of the structure shown in Figure 1.

Rietveld profile refinement of this structural model against neutron powder diffraction data collected from $K_4Fe_3F_{12}$ at 298 K gives an excellent fit (Figure 2), with refined structural parameters in excellent agreement with those determined from single-crystal X-ray data, as detailed in the Supporting Information (SI).

**Table 1. Crystallographic Data for $K_4Fe_3F_{12}$**

| parameter | $K_4Fe_3F_{12}$ |
|---|---|
| fw | 551.95 |
| $T$ (K) | 296(2) |
| $\lambda$ (Å) | 0.71073 |
| cryst syst | trigonal |
| space group | $R\bar{3}m$ (No. 166) |
| $a$ (Å) | 5.7649(9) |
| $b$ (Å) | 5.7649(9) |
| $c$ (Å) | 28.086(9) |
| $V$ (Å$^3$) | 808.36(3) |
| $Z$ | 3 |
| $\rho_{calcd}$ (g/cm$^3$) | 3.401 |
| $\mu$ (mm$^{-1}$) | 5.674 |
| $2\theta_{max}$ (deg) | 57.94 |
| $R$(int) | 0.0402 |
| GOF | 1.106 |
| $R(F)^a$ | 0.0188 |
| $R_w(F_o^2)^b$ | 0.0579 |

$^aR(F) = \sum||F_o| - |F_c||/\sum|F_o|$. $^bR_w(F_o^2) = [\sum w(F_o^2 - F_c^2)^2/\sum w(F_o^2)^2]^{1/2}$.

**Table 2. Atomic Coordinates for $K_4Fe_3F_{12}$**

| atom | $x$ | $y$ | $z$ | $U_{eq}$ (Å$^2$)$^a$ |
|---|---|---|---|---|
| K(1) | $^2/_3$ | $^1/_3$ | 0.0458(1) | 0.0171(2) |
| K(2) | 0 | 0 | 0.1399(3) | 0.0239(3) |
| Fe(1) ($Fe^{2+}$) | 0 | 0 | 0 | 0.0102(2) |
| Fe(2) ($Fe^{3+}$) | $^1/_3$ | $^2/_3$ | 0.0847(1) | 0.0105(1) |
| F(1) | 0.6507(2) | 0.8253(1) | 0.0403(1) | 0.0212(4) |
| F(2) | 0.4901(1) | 0.9881(3) | 0.1184(3) | 0.0214(3) |

$^aU_{eq}$ is defined as one-third of the trace of the orthogonal $U_{ij}$ tensor.

**Table 3. Selected Bond Distances and Angles and Bond Valence Sums for $K_4Fe_3F_{12}$**

| cation | anion | bond length (Å) | BVS |
|---|---|---|---|
| K(1) | F(1) | 2.888(1) (×6) | 1.27 |
| | F(1) | 2.891(2) (×3) | |
| | F(2) | 2.671(2) (×3) | |
| K(2) | F(2) | 2.946(1) (×6) | 0.867 |
| | F(2) | 2.721(2) (×3) | |
| Fe(1) | F(1) | 2.079(1) (×6) | 1.88 |
| Fe(2) | F(1) | 2.016(1) (×3) | 3.02 |
| | F(2) | 1.864(1) (×3) | |
| | angle (deg) | | angle (deg) |
| F(1)–Fe(1)–F(1) | 86.83(5) | F(2)–Fe(2)–F(2) | 96.46(5) |
| F(1)–Fe(1)–F(1) | 93.17(5) | F(1)–Fe(2)–F(2) | 85.78(6) |
| F(1)–Fe(1)–F(1) | 180.0 | F(1)–Fe(2)–F(2) | 88.62(4) |
| | | F(1)–Fe(2)–F(2) | 172.35(6) |
| | | Fe(1)–F(1)–Fe(2) | 174.79(7) |

**Magnetic Characterization.** Zero-field-cooled (ZFC) and field-cooled (FC) magnetization data, collected from $K_4Fe_3F_{12}$ in an applied field of 100 Oe, diverge below $T \sim 120$ K, as shown in Figure 3, indicative of a magnetic transition at this temperature. A magnetization-field isotherm collected at 10 K from $K_4Fe_3F_{12}$ (Figure 4) exhibits hysteresis with a coercive field of 1750 Oe and a saturated moment of 5.46 $\mu_B$ per formula unit, indicating that the low-temperature magnetic state has a spontaneous magnetization, consistent with ferromagnetic or ferrimagnetic behavior.



DOI: 10.1021/acs.inorgchem.5b01006
*Inorg. Chem.* 2015, 54, 6647–6652

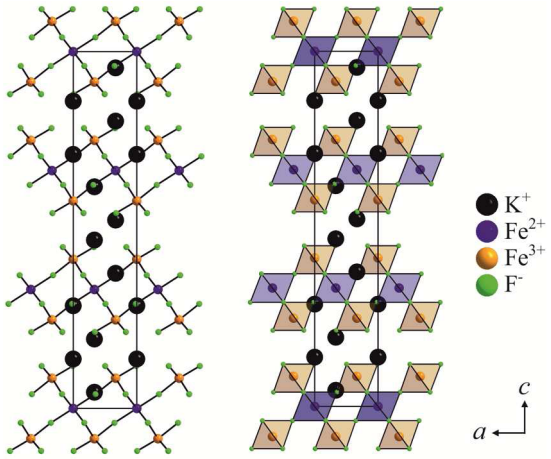


**Figure 1.** Ball-and-stick and polyhedral representations of $K_4Fe_3F_{12}$ in the *ac* plane.

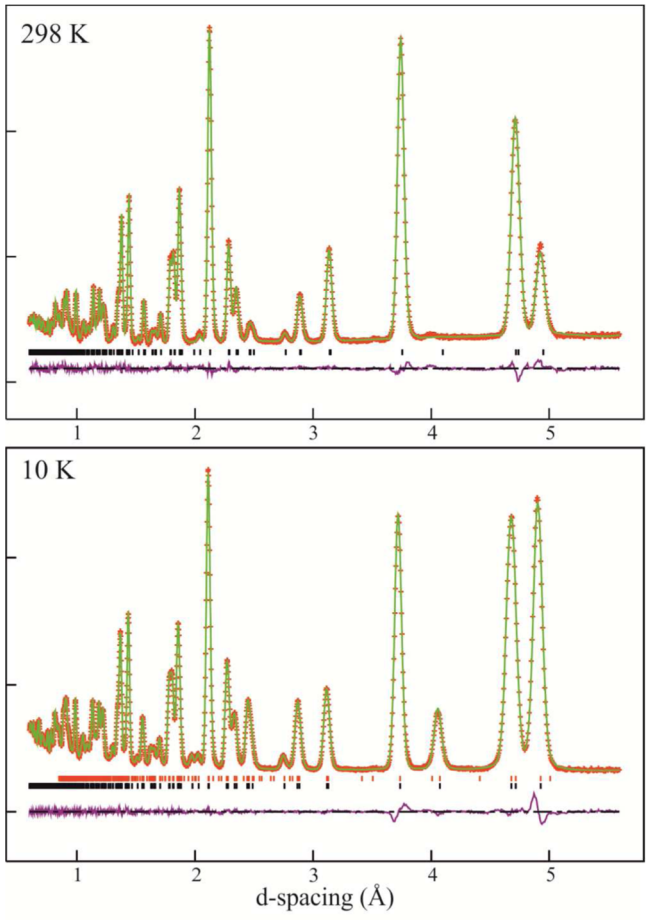


**Figure 2.** Comparison of the observed calculated and difference plots from the nuclear and magnetic structural refinements of $K_4Fe_3F_{12}$ against neutron powder diffraction data (35° bank) collected at 298 K (top) and 10 K (bottom).

To investigate the nature of the low-temperature magnetic state, neutron powder diffraction data were collected from $K_4Fe_3F_{12}$ at 10 K. These low-temperature diffraction data exhibit a dramatically different intensity distribution compared to analogous data collected at 298 K, as shown in Figure 2, indicating the presence of an ordered magnetic lattice. The magnetic diffraction features observed in the 10 K neutron

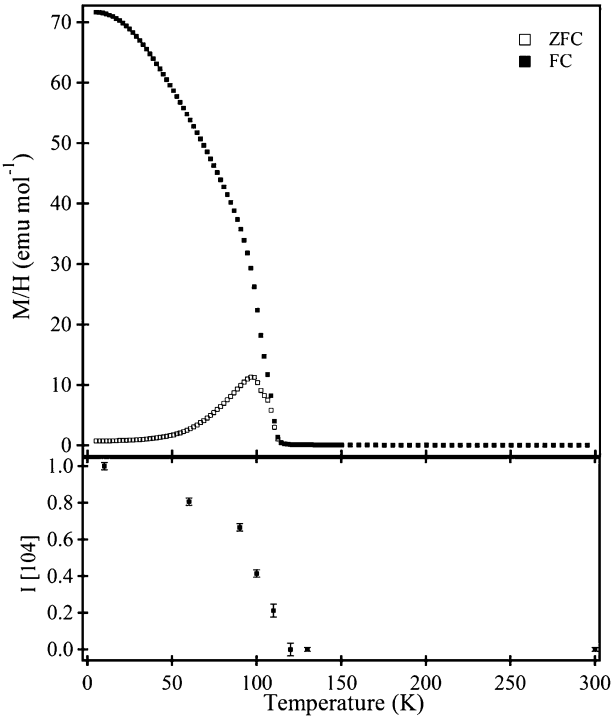


**Figure 3.** Plots as a function of the temperature of ZFC and FC magnetization data in an applied field of 100 Oe (top) and the normalized intensity of the [104] magnetic scattering peak in neutron diffraction data (bottom), collected from $K_4Fe_3F_{12}$.

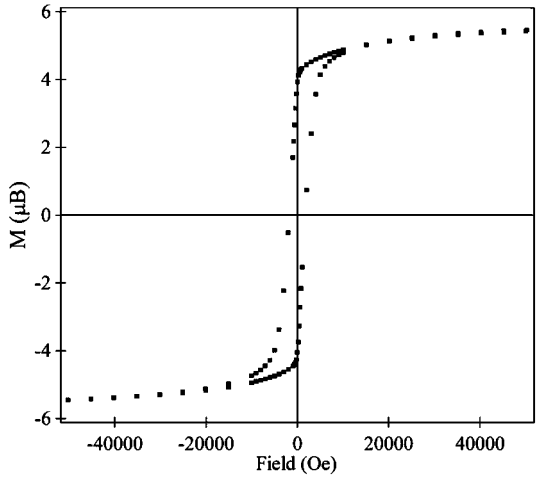


**Figure 4.** Magnetization-field isotherm collected from $K_4Fe_3F_{12}$ at 10 K.

powder diffraction data were readily indexed using the crystallographic unit cell, indicating a magnetic propagation vector, **k** = 0. Thus, a magnetic model was constructed consisting of two independent, ferromagnetic sublattices, one located on the Fe(1) crystallographic sites and the other on the Fe(2) crystallographic sites. This model was refined against the 10 K neutron powder diffraction data set (in combination with a nuclear model based on the room temperature crystal structure of $K_4Fe_3F_{12}$) with the local moment of each sublattice allowed to refine independently. The refinement converged rapidly to give a good fit to the data ($\chi^2$ = 5.73) with ordered moments of 4.24(9) and 4.55(11) $\mu_B$ located on the Fe(1) and Fe(2) sites, respectively, aligned in an approximately


DOI: 10.1021/acs.inorgchem.5b01006
*Inorg. Chem.* 2015, 54, 6647−6652

antiparallel manner, as described in Table 4 and shown in Figure 5, to yield a net moment of 5.41 $\mu_B$ per formula unit, in good agreement with the magnetization data. Subsequent to the refinement of this magnetic model, a magnetic symmetry analysis, using the SARAh code,[19] was performed to confirm that the refined magnetic model is consistent with the crystallographic symmetry and that there are no other symmetry-allowed magnetic models, which give an equivalently good fit to the data. Full details of the low-temperature nuclear and magnetic structural refinement of $K_4Fe_3F_{12}$ are given in the SI.

**Table 4. Ordered Local Magnetic Moments ($\mu_B$) of the Iron Centers in $K_4Fe_3F_{12}$, Determined by Refinement against Neutron Powder Diffraction Data Collected at 10 K**

| atom | $M_x$ | $M_y$ | $M_z$ | total |
|---|---|---|---|---|
| Fe(1) | 4.21(9) | 0 | 0.51(4) | 4.24(9) |
| Fe(2) | −3.98(8) | 0 | −2.21(9) | 4.55(11) |
| Fe(1) + 2Fe(2) | −3.75 | 0 | −3.91 | 5.41 |

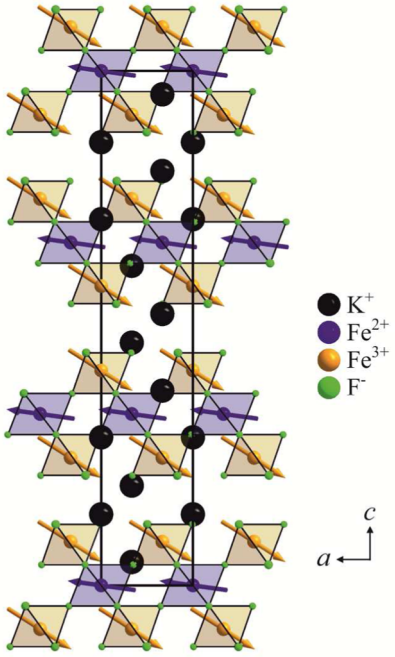


**Figure 5.** Magnetic structure of $K_4Fe_3F_{12}$ refined against neutron powder diffraction data collected at 10 K viewed in the *ac* plane.

Upon warming from 10 K, the intensity of the magnetic scattering in neutron powder diffraction data sets declined, behavior that is most easily quantified by following the intensity of the [104] "magnetic only" diffraction peak ($d$ = 4.05 Å) as a function of the temperature. As shown in Figure 3, it can be seen that the intensity of the [104] reflection declines to zero at $T \sim 120$ K, such that neutron powder diffraction data collected at 120 K could be fitted well by only the nuclear model, confirming that magnetic transition occurs at approximately this temperature.

## DISCUSSION

**Synthesis and Structure.** The layered, B-cation-deficient, perovskite structure adopted by $K_4Fe_3F_{12}$ is, to the best of our knowledge, unique among extended metal fluoride phases and is, as such, the first reported example of a fluoride phase adopting such a structural framework. The lack of structurally analogous fluoride phases is surprising (but could just arise from the relatively small number of complex transition-metal fluorides that have been prepared to date) because structurally analogous oxide phases are relatively common. This is particularly true when early transition metals in their group oxidation states ($Ti^{4+}$, $Nb^{5+}$, and $Ta^{5+}$) are located on the B sites of the $A_4B_3O_{12}$ framework, forming phases such as $La_4Ti_3O_{12}$, $LaSr_3Nb_3O_{12}$, or $LaBa_3Ta_3O_{12}$.[18,20,21] Indeed, the layered, cation-deficient framework appears to be sufficiently favorable to allow a large series of structurally related, cation-deficient $A_nB_{n-1}O_{3n}$ oxide phases to be prepared by adjusting the identity and concentration of the A and B cations to achieve charge balance, as observed for the series $LaBa_3Nb_3O_{12}$, $LaBa_4Nb_3TiO_{15}$, and $LaBa_5Nb_3Ti_2O_{18}$, for example.[22−24]

The large number of $A_nB_{n-1}O_{3n}$ oxide phases that can be prepared in this structural series suggests that a structurally analogous series of complex fluorides with $A_nB_{n-1}F_{3n}$ (A = Na, K, Rb; B = Fe, Co, Ni) compositions may also be preparable, an idea supported by the observation that a number of structurally related fluoride phases with $n$ = 3 compositions, containing divalent transition metals, are already known (e.g., $Ba_2RbFe_2F_9$, $Ba_2CsCo_2F_9$, and $Ba_2KNi_2F_9$).[25] Thus, if transition-metal oxidation states can be effectively controlled during the synthesis, a range of new layered, cation-deficient, mixed-valent fluorides could be prepared.

Close inspection of the room-temperature structure of $K_4Fe_3F_{12}$ reveals significantly different Fe−F bond lengths for the two crystallographically distinct iron centers (Table 3). BVSs[26] calculated for these two centers are consistent with the $Fe^{2+}/Fe^{3+}$ charge order, as shown in Figure 1. The $Fe^{2+}/Fe^{3+}$ charge order has been observed previously in a number of complex iron fluoride phases, such as $RbFe_2F_6$ and $K_3Fe_5F_{15}$,[27,28] where the ratio of $Fe^{2+}/Fe^{3+}$ is commensurate with the crystallographic multiplicity of the different iron centers within their structures. This condition also exists for $K_4Fe_3F_{12}$, facilitating a strong charge order at room temperature, and would be expected to be maintained for any additional $K_nFe_{n-1}F_{3n}$ phases subsequently prepared.

As an aside, it should be noted that the manganese analogue of $K_4Fe_3F_{12}$, $K_4Mn_3F_{12}$, also adopts a charge-ordered, cation-deficient perovskite structure.[29] However, in contrast to $K_4Fe_3F_{12}$, the B-cation vacancies in $K_4Mn_3F_{12}$ are isolated, rather than arranged, in layers of trigonal symmetry, resulting in a tetragonal rather than rhombohedral crystal symmetry for $K_4Mn_3F_{12}$. This structural difference can be attributed to the need to accommodate the axially elongated, Jahn−Teller-distorted, $Mn^{3+}F_6$ centers, in a charge-ordered and orbitally ordered array, which is not possible while maintaining the 3-fold rotational symmetry of the layered structure of $K_4Fe_3F_{12}$. Thus, we can see that the structure adopted by $K_4Fe_3F_{12}$ is not just a product of the stoichiometry of the phase but also the spherical and near-spherical nature of the $Fe^{3+}$ and $Fe^{2+}$ cations.

**Magnetic Behavior.** Magnetization and neutron powder diffraction data show that, upon cooling below 120 K, $K_4Fe_3F_{12}$ adopts a magnetically ordered state in which the $Fe^{3+}$ and $Fe^{2+}$ spins are aligned in an approximately antiparallel manner to each other, as shown in Figure 5. Considering the strong $Fe^{2+}/Fe^{3+}$ charge order and the layered structure exhibited by $K_4Fe_3F_{12}$, the magnetic coupling interactions in the material are dominated by a $Fe^{2+}(3d\sigma)^1-F(2p)^2-Fe^{3+}(3d\sigma)^1$ superexchange (where $3d\sigma$ refers to either of the $3d_{z^2}$ or $3d_{x^2-y^2}$


DOI: 10.1021/acs.inorgchem.5b01006
Inorg. Chem. 2015, 54, 6647−6652

orbitals) through the Fe(1)−F(1)−Fe(2) linkage. This exchange coupling is expected to be strongly antiferromagnetic, according to the Goodenough−Kanamouri rules,[30] consistent with the observed magnetic structure.

The local ordered moments of the Fe(1) and Fe(2) crystallographic sites [Fe(1) = 4.24(9) $\mu_B$; Fe(2) = 4.55(11) $\mu_B$], determined from the low-temperature neutron diffraction data, fall within the ranges expected for $Fe^{2+}$ and $Fe^{3+}$, respectively, confirming the charge-ordered picture derived from the crystallographic structure. It should be noted that while the spin-only values for $Fe^{2+}$ and $Fe^{3+}$ are 4 and 5 $\mu_B$, respectively, the $d^6t_{2g}{}^4e_g{}^2$ state of $Fe^{2+}$ can have an appreciable unquenched orbital contribution to its moment. For example, the local moment of $Fe^{2+}$ in $FeF_2$ is observed to be ∼4.48 $\mu_B$.[31,32] If the local moments of the Fe(1) and Fe(2) centers were arranged in a strictly antiparallel manner, the purely ferrimagnetic arrangement would yield a net magnetization of 4.86 $\mu_B$ per formula unit. However, there is a slight canting of the two magnetic sublattices, raising the net moment to 5.41 $\mu_B$. This weak ferromagnetic component of the magnetic structure can be attributed to a slight tightening of the Fe(1)−F(1)−Fe(2) bond angle from 180°, introducing a weak ferromagnetic contribution to the exchange coupling.

## CONCLUSION

Preparing paramagnetic transition-metal fluoride phases that are structurally analogous to diamagnetic transition-metal oxide phases offers an efficient route to the discovery of novel magnetic materials. In this instance, the preparation of $K_4Fe_3F_{12}$ (structurally analogous to diamagnetic $La_3Ti_3O_{12}$) reveals that this phase adopts a pseudoferrimagnetic state below 120 K with a significant spontaneous magnetization and magnetic coercivity. This magnetic behavior arises from the combination of a layered crystal structure and strong $Fe^{2+}/Fe^{3+}$ charge order. Given the prevalence of transition-metal oxide phases that adopt related layered, cation-deficient perovskite structures, it is likely that $K_4Fe_3F_{12}$ is the first in a series of novel magnetic fluoride materials based on this structural family.

## ASSOCIATED CONTENT

### Supporting Information

X-ray crystallographic data in CIF format and structural parameters and observed calculated and difference plots from the nuclear and magnetic structural refinement of $K_4Fe_3F_{12}$ against neutron powder diffraction data collected at 298 and 10 K. The Supporting Information is available free of charge on the ACS Publications website at DOI: 10.1021/acs.inorgchem.5b01006.

## AUTHOR INFORMATION

### Corresponding Authors

*E-mail: psh@uh.edu.

*E-mail: michael.hayward@chem.ox.ac.uk.

### Author Contributions

The manuscript was written through contributions of all authors.

### Notes

The authors declare no competing financial interest.

## ACKNOWLEDGMENTS

We thank I. da Silva for assistance in collecting the neutron powder diffraction data. Experiments at the ISIS pulsed neutron facility were supported by a beam-time allocation from the Science and Technology Facilities Council. S.W.K. and P.S.H. thank the Welch Foundation (Grant E-1457) for support.

## REFERENCES

(1) Hagenmuller, P. *Inorganic Solid Fluorides*; Academic Press: Orlando, FL, 1985.
(2) Behera, B.; Nayak, P.; Choudhary, R. N. P. *Mater. Lett.* **2005**, *59*, 3489.
(3) Blinc, R.; Tavcar, G.; Zemva, B.; Hanzel, D.; Cevc, P.; Filipic, C.; Levstik, A.; Jaglicic, Z.; Trontelj, Z.; Dalal, N.; Ramachandran, V.; Nellutla, S.; Scott, J. F. *J. Appl. Phys.* **2008**, *103*, 74114.
(4) Blinc, R.; Tavcar, G.; Zemva, B.; Goreshnik, E.; Hanzel, D.; Cevc, P.; Potocnik, A.; Laguta, V.; Trontelj, Z.; Jaglicic, Z.; Scott, J. F. *J. Appl. Phys.* **2009**, *106*, 23924.
(5) Blinc, R.; Cevc, P.; Potocnik, A.; Zemva, B.; Goreshnik, E.; Hanzel, D.; Gregorovic, A.; Trontelj, Z.; Jaglicic, Z.; Laguta, V.; Perovic, M.; Dalal, N. S.; Scott, J. F. *J. Appl. Phys.* **2010**, *107*, 43511.
(6) Cava, R. J.; Roth, R. S. *J. Solid State Chem.* **1981**, *36*, 139.
(7) Jian, L.; Wayman, C. M. *J. Am. Ceram. Soc.* **1997**, *80*, 803.
(8) Cordrey, K. J.; Stanczyk, M.; Dixoon, C. A. L.; Knight, K. S.; Gardner, J.; Morrison, F. D.; Lightfoot, P. *Dalton Trans.* **2015**, *44*, 10673.
(9) Cox, D. E.; Eibschut, M.; Guggenhe, H.; Holmes, L. *J. Appl. Phys.* **1970**, *41*, 943.
(10) Keve, E. T.; Abrahams, S. C.; Bernstei, J. L. *J. Chem. Phys.* **1969**, *51*, 4928.
(11) Keve, E. T.; Abrahams, S. C.; Bernstei, J. L. *J. Chem. Phys.* **1970**, *53*, 3279.
(12) Kim, S. W.; Chang, H. Y.; Halasyamani, P. S. *J. Am. Chem. Soc.* **2010**, *132*, 17684.
(13) *SAINT, Program for Area Detector Absorption Correction*, 4.05; Siemens Analytical X-ray Systems: Madison, WI, 1995.
(14) Sheldrick, G. M. *SHELXS-97, A program for automatic solution of crystal structures*; University of Goettingen: Goettingen, Germany, 1997.
(15) Sheldrick, G. M. *SHELXS-97, A program for Crystal Structure Refinement*; University of Goettingen: Goettingen, Germany, 1997.
(16) Farrugia, L. J. *J. Appl. Crystallogr.* **1999**, *32*, 837.
(17) Larson, A. C.; Von Dreele, R. B. *General Structure Analysis System*; Los Alamos National Laboratory: Los Alamos, NM, 2000; Report LAUR 86-748.
(18) Konstantinov, P.; Krezhov, K.; Svab, E.; Meszaros, G.; Torok, G. *Physica B* **2000**, *276*, 260.
(19) Wills, A. S. *Physica B* **2000**, *276*, 680.
(20) Tabacaru, C.; Aguadero, A.; Sanz, J.; Chinelatto, A. L.; Thursfield, A.; Perez-Coll, D.; Metcalfe, I. S.; Fernandez-Diaz, M. T.; Mather, G. C. *Solid State Ionics* **2013**, *253*, 239.
(21) Zhang, H.; Wu, Y. M.; Meng, S. S.; Fang, L. *J. Alloys Compd.* **2008**, *460*, 460.
(22) Rother, H. J.; Kemmlersack, S.; Treiber, U.; Cyris, W. R. *Z. Anorg. Allg. Chem.* **1980**, *466*, 131.
(23) De Paoli, J. M.; Alonso, J. A.; Carbonio, R. E. *J. Phys. Chem. Solids* **2006**, *67*, 1558.
(24) Zhang, H.; Fang, L.; Dronskowski, R.; Muller, P.; Yuan, R. Z. *J. Solid State Chem.* **2004**, *177*, 4007.
(25) Herdtweck, E.; Kummer, S.; Babel, D. *Eur. J. Solid State Inorg. Chem.* **1991**, *28*, 959.
(26) Brese, N. E.; O'Keeffee, M. *Acta Crystallogr., Sect. B: Struct. Sci.* **1991**, *B47*, 192.
(27) Kim, S. W.; Kim, S. H.; Halasyamani, P. S.; Green, M. A.; Bhatti, K. P.; Leighton, C.; Das, H.; Fennie, C. J. *Chem. Sci.* **2012**, *3*, 741.
(28) Fabbrici, S.; Montanari, E.; Righi, L.; Calestani, G.; Migliori, A. *Chem. Mater.* **2004**, *16*, 3007.
(29) Frenzen, G.; Kummer, S.; Massa, W.; Babel, D. *Z. Anorg. Allg. Chem.* **1987**, *553*, 75.
(30) Goodenough, J. B. *Magnetism and the Chemical Bond*; Wiley: New York, 1963.



DOI: 10.1021/acs.inorgchem.5b01006
*Inorg. Chem.* 2015, 54, 6647−6652

(31) Ohlmann, R. C.; Tinkham, M. *Phys. Rev.* **1961**, *123*, 425.
(32) Strempfer, J.; Rutt, U.; Jauch, W. *Phys. Rev. Lett.* **2001**, *86*, 3152.



DOI: 10.1021/acs.inorgchem.5b01006
*Inorg. Chem.* 2015, 54, 6647−6652